Atomistic Modeling of Two-Dimensional Electronic Spectra and Excited-State Dynamics for a Light Harvesting 2 Complex

ARTICLE *in* THE JOURNAL OF PHYSICAL CHEMISTRY B · JANUARY 2015

Impact Factor: 3.3 · DOI: 10.1021/jp509247p · Source: PubMed

5 AUTHORS, INCLUDING:

Jignesh Prajapati
Jacobs University
2 PUBLICATIONS **4** CITATIONS
SEE PROFILE

Ulrich Kleinekathöfer
Jacobs University
117 PUBLICATIONS **2,054** CITATIONS
SEE PROFILE

Thomas La Cour Jansen
University of Groningen
78 PUBLICATIONS **1,716** CITATIONS
SEE PROFILE

THE JOURNAL OF PHYSICAL CHEMISTRY B

Article

pubs.acs.org/JPCB

Atomistic Modeling of Two-Dimensional Electronic Spectra and Excited-State Dynamics for a Light Harvesting 2 Complex

C. P. van der Vegte,[†] J. D. Prajapati,[‡] U. Kleinekathöfer,[‡] J. Knoester,[†] and T. L. C. Jansen*[,†]

[†]Zernike Institute for Advanced Materials, University of Groningen, Nijenborgh 4, 9747 AG Groningen, The Netherlands

[‡]School of Engineering and Science, Jacobs University Bremen, Campus Ring 1, 28759 Bremen, Germany

ABSTRACT: The Light Harvesting 2 (LH2) complex is a vital part of the photosystem of purple bacteria. It is responsible for the absorption of light and transport of the resulting excitations to the reaction center in a highly efficient manner. A general description of the chromophores and the interaction with their local environment is crucial to understand this highly efficient energy transport. Here we include this interaction in an atomistic way using mixed quantum-classical (molecular dynamics) simulations of spectra. In particular, we present the first atomistic simulation of nonlinear optical spectra for LH2 and use it to study the energy transport within the complex. We show that the frequency distributions of the pigments strongly depend on their positions with respect to the protein scaffold and dynamics of their local environment. Furthermore, we show that although the pigments are closely packed the transition frequencies of neighboring pigments are essentially uncorrelated. We present the simulated linear absorption spectra for the LH2 complex and provide a detailed explanation of the states responsible for the observed two-band structure. Finally, we discuss the energy transfer within the complex by analyzing population transfer calculations and 2D spectra for different waiting times. We conclude that the energy transfer from the B800 ring to the B850 ring is mediated by intermediate states that are delocalized over both rings, allowing for a stepwise downhill energy transport.

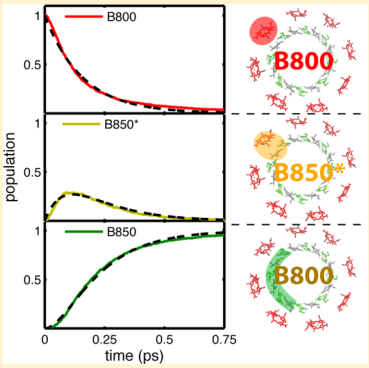

INTRODUCTION

The photosystem of purple bacteria is very efficient in turning sunlight into chemical energy.[1] This energy conversion occurs in the reaction center (RC), where the charge separation takes place. The RC is surrounded by antenna complexes Light Harvesting 1 (LH1) and Light Harvesting 2 (LH2) to enhance the absorption cross section of the photosystem.[2,3] These antenna systems are responsible for the absorption of light and the transfer of the excitation to the RC. For efficient light harvesting it is crucial that this energy transfer is fast so that the excitation reaches the RC before relaxation occurs. A general description of the pigments and the interaction with their local environment is essential to understand this highly efficient energy transport. Here we present a mixed quantum-classical simulation method for calculating (non)linear spectra where the interaction between the pigments and their environment is included in an atomistic way. We apply the method to study energy transfer within a single LH2 complex and show that the nature of states within the complex allows for a fast downhill energy transfer.

From high-resolution studies the structure of the LH2 complex is known in great detail.[4−6] The complex is composed of pigments mounted on proteins, and it is the electrostatic interactions between the pigments that mediates the energy transfer. The LH2 complex comprises either eight or nine identical transmembrane protein structures leading to an eight-[6] or nine-fold[5] symmetry, depending on the species of purple bacteria. In Figure 1 a schematic picture is shown for the LH2

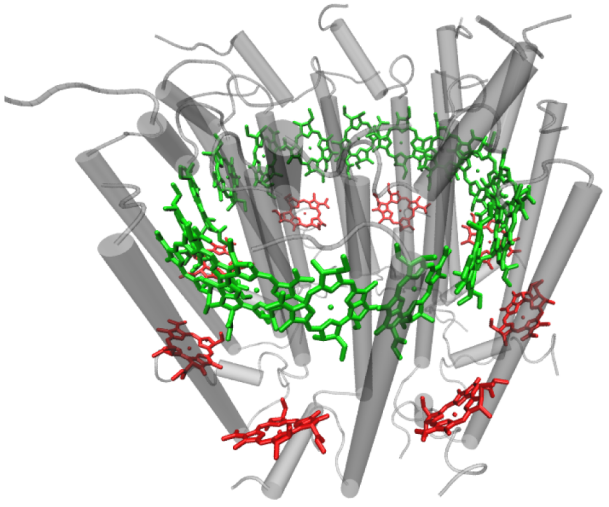

Figure 1. Schematic overview of the LH2 complex of *Rhodospirillum molischianum*. The BChla chromophores form two concentric rings mounted on the protein scaffold. The B850 ring colored in green contains twice as many chromophores as the B800 ring shown in red. The Figure was rendered using VMD.[96]

Received: September 12, 2014
Revised: December 22, 2014
Published: January 2, 2015

DOI: 10.1021/jp509247p
J. Phys. Chem. B 2015, 119, 1302−1313

complex of *Rhodospirillum molischianum*, which has an eight-fold symmetry. Each of the transmembrane protein binds three optically active bacteriochlorophyll a (BChla) molecules and one or two carotenoids. In this study we focus on the optical response of the BChla pigments. They form two concentric rings that are often referred to as the B850 ring and B800 ring due to their absorption bands around 850 and 800 nm at room temperature.[7]

The study of the LH2 complex greatly intensified both experimentally and theoretically after the high-resolution structure was determined.[4−6] Low-temperature fluorescence spectroscopy experiments allow us to study single LH2 complexes and reveal the dense electronic structure that in ensemble studies is washed away due to disorder.[8−13] Energy transfer within the complex has been studied using two-dimensional electronic spectroscopy (2DES) experiments[14,15] on ensembles of LH2 complexes.[16−18] In such experiments three ultrafast laser pulses are applied to the system with respective time delays t_1 and t_2, during which the system is in a coherence and population, respectively. A radiated signal is measured at a time t_3 after the third laser pulse, using a reference pulse. By Fourier transforming over the time delays t_1 and t_3 a correlation spectrum as a function of ω_1 and ω_3, respectively, is obtained for a chosen waiting time t_2. Such 2D correlation spectra are sensitive to both population transfer and structural dynamics that occur during the waiting time.[15,19] The energy transfer between two states, for example, is comprised in the 2D spectra through the growth of a cross peak at the location where ω_1 is equal to the energy of the initial state and ω_3 is equal to the energy of the state to which the energy is transferred. By studying the growth of such cross peaks, as a function of the waiting time, detailed information on the energy transfer within the system is obtained. The 2D spectra are complicated to understand, however, due to the complex nature of the excited states and overlapping peaks. In the 2D spectra of antenna complexes like the Fenna−Matthews−Olson (FMO) complex and LH2, for example, oscillations that remain for hundreds of femtoseconds have been observed.[16,20−22] It has been argued that the oscillations originate from quantum coherences between excitonic states, protected from dephasing by the protein environment, and that the coherent transport between these states is responsible for the efficient energy transfer.[16,21] Although coherent transport may indeed be responsible for the observed oscillations, it has also been proposed that these oscillations arise from underdamped vibrational modes of the environment.[23,24] To interpret the 2D spectra and disentangle between such effects, theoretical models and simulations that include a detailed description of the pigments and the interaction with their local environment are crucially needed. So far, theoretical models and simulations have been used to calculate the absorption spectra,[25−27] fluorescence spectra,[9,28] population transfer,[26,27,29−36] and more recently 2D spectra for zero waiting times[37] for LH2. The interaction between the chromophores and their environment in these models is often included in a simplified stochastic way, where the used parameters are fitted to experimental data.

In this study we describe the interaction between the pigments and their environment in an atomistic way using classical molecular dynamics simulations. The pigment protein complex is embedded in a lipid bilayer membrane surrounded by water. The electronic excitations of the BChla pigments are described quantum mechanically, and the parameters for the transition frequencies, transition dipoles, and couplings are determined by the positions of all classical atoms in the simulation box. Previously, similar mixed quantum-classical simulations of linear spectra and spectral densities have been performed for light harvesting complexes using time-dependent density functional theory and semiempirical electronic structure calculations to determine the transition frequencies.[38−44] Such quantum-chemical calculations are, however, computationally demanding and, therefore, extremely expensive for calculations of 2D spectra.[39] Within this study, we use the much cheaper charge density coupling method[25,45−47] to determine the transition frequencies. We calculate the linear spectra, energy transfer in the LH2 complex, and present the first 2D spectra for LH2, simulated using an atomistic description of the environment. Within our simulations the quantum and classical subsystems are coupled to each other in a self-consistent way using the surface-hopping method.[48−50] This method accounts for the Stokes shift and leads to a Boltzmann distribution within the quantum system in equilibrium, which is crucial when dealing with electronic systems where the energy separation between states is comparable to or larger than k_BT.[48−50] Semiempirical electronic structure calculations usually assume a ground-state trajectory for the classical system and are unable to describe these effects. Some exceptions are refs 51 and 52. The method presented here can readily be applied to other light harvesting systems like LH1, photosystem II, and FMO.

The remainder of this paper is outlined as follows. In the Theory section we briefly describe the simulation setup and the method for calculating the (non)linear spectra using the surface-hopping method. In the Results section we present the distribution functions of the transition frequencies, transition dipoles, and couplings within the system. In addition, we show that the protein-induced correlations between transition frequencies of neighboring pigments are insignificant for LH2 and cannot be used to explain the beating signals observed in the 2D spectra. Furthermore, we present the simulated linear spectra and analyze the nature of the states that are responsible for the absorption in the B800 and B850 bands. Finally, we show our results for the energy transfer and 2D spectra calculations on LH2. We demonstrate that energy transfer can rapidly occur from the B800 band to the B850 band due to the highly delocalized nature of the electronic states.

THEORY

We calculate the (non)linear optical response of the LH2 complex using an atomistic mixed quantum-classical molecular dynamics simulations. The quantum and classical subsystem are coupled to each other in a self-consistent way using the surface-hopping method.[48−50] The molecular dynamics simulation box consists of 114 011 atoms and is identical to the one used and described in ref 38. The simulation box contains a single *Rs. molishianum* LH2 complex arranged according to the crystal structure.[6] The pigment−protein complex is embedded in a 1-palmitoyl-2-oleoyl-*sn*-glycero-3-phosphocholine (POPC) lipid bilayer surrounded by ∼30 Å of water molecules on both sides. We are interested in the spectral region of the Q_y transition of the BChla pigments and therefore treat their electronic excitation quantum mechanically and all other degrees of freedom classically. The excited states of the carotenoids are not included in the quantum subsystem because their transitions are much higher in energy than the Q_y transitions[27] of the BChla pigments and therefore do not play a role in the energy transport between the B800 and B850 ring. Because of the Coulomb interactions the presence of the carotenoids,

DOI: 10.1021/jp509247p
J. Phys. Chem. B 2015, 119, 1302−1313

however, does influence the directions and magnitudes of the transition dipoles of the BChla pigments and therefore the couplings between them.[27,53]

The 24 BChla chromophores are considered as coupled two-level quantum systems and are described by the Frenkel exciton Hamiltonian. The transition frequencies, transition dipoles, and excitonic couplings depend on the positions of all the atoms in the simulation box (chromophores themselves and their environment). We use the charge density coupling method[25,45−47] to calculate the transition frequencies of the chromophores, which is a first-order perturbation theory in the intermolecular Coulomb interaction. The transition frequency of a chromophore i in this approach is given by

$$\omega_i = \omega_0 + \frac{1}{\varepsilon}\sum_{k=1}^{N_i}\sum_{l=1}^{N_{env}}\frac{\Delta q_{ik}^{eg} q_l}{|\vec{r}_{ik} - \vec{r}_l|} \quad (1)$$

Here ω_0 is the transition frequency of the chromophore in the absence of an environment and is equal for all 24 chemically identical BChla pigments. It is value is chosen to be 10 900 cm^{-1} to match the overall position of the spectra compared with experimental data. The second term describes the influence of the environment on the pigment's transition frequency. This term is the difference between the Coulomb interaction energy with the environment, when the pigment is in the ground and the excited states. Δq_{ik}^{eg} denotes the charge difference of the chromophores kth atom between the excited and ground states. We use the values reported in ref 46 calculated at the TDDFT/B3LYP/6-31G* level of theory. The partial charges of the chromophores in the ground state in our simulation are, however, determined by the force field[54] and are different from the ones calculated in ref 46. For each atom, k, of the chromophore, i, the difference in Coulomb interaction energy is calculated by summing over all contributions of the N_{env} charged atoms in the simulation box. Screening effects of the local environment on the transition frequencies can be included via the effective dielectric constant, ε.[45,55] We use the transition charge electrostatic potential (TrEsp) method[46,56] to calculate the transition dipoles of the chromophores and the excitonic couplings between them for a configuration of the simulation box. In this method the transition densities of the chromophores are represented by partial transition charges located at the atoms that form the chromophore and are provided by ref 46 as well. The transition dipole of a chromophore i is given by

$$\vec{\mu}_i = \sum_{k=1}^{N_i} q_{ik}(1, 0)\vec{r}_{ik} \quad (2)$$

where the sum is over all atomic partial transition charges $q_{ik}(1,0)$ of the pigment with coordinates $\vec{r}_{ik}$. In the TrEsp method the excitonic coupling between two chromophores i and j is obtained by the electrostatic interaction between their transition charges

$$J_{ij} = \frac{1}{\varepsilon}\sum_{k=1}^{N_i}\sum_{l=1}^{N_j}\frac{q_{ik}(1, 0)q_{jk}(1, 0)}{|\vec{r}_{ik} - \vec{r}_{jl}|} \quad (3)$$

The absolute values of the transition charges are typically rescaled to match an observable.[46] Peviously, the transition charges were rescaled with a factor in the range 0.63 to 0.75 to match the vacuum transition dipole moment of 6.1 D of the BChla chromophores.[46] A rescaling factor of 0.81 has also been used to match the expected excitonic couplings between nearest neighbor pigments in the B850 ring of around 250−300 cm^{-1}.[25] Here we rescale the couplings by a factor of 0.7 to reproduce the energy splitting between the two bands observed in the linear spectrum. Polarization effects on the couplings between pigments can be included via the dielectric constant, ε, which is system-dependent. Several distance-dependent functions have been proposed as well as functions, which depend on the relative orientation of the chromophores.[57] Hsu et al.[58] showed that the couplings between two chromophores when embedded in a medium with a dielectric constant of $\varepsilon = 2$ can differ between 80 and 110% of the coupling between them in a vacuum, depending on their relative orientation. The coupling strengths directly influence the excitonic splittings, determining the peak positions to which we matched the transition charges already. Therefore, we use a constant value for the dielectric constant of $\varepsilon = 1$ like was done in refs 25 and 46.

In the Frenkel exciton Hamiltonian the pigments are described as coupled two-level systems, neglecting the intramolecular vibrations because in a previous study they were found to give a negligible contribution to the spectral density of BChla.[59] These vibrational modes can be included using the Holstein Hamiltonian for the coupling to the dominant modes, like was done in ref 60, or by including them in the spectral density using semiempirical electronic structure calculations.[38,39] This, however, significantly increases the computational cost for calculating the nonlinear spectra.

The state of the classical subsystem is defined by the positions and velocities of all 114 011 atoms in the simulation box. The potential energy surface a classical atom feels is determined by the positions of all of the other atoms in the simulation box and the state of the quantum system. The forces between atoms are computed using the Gromacs 4.5.5 distribution[61] and are determined by the force field. The CHARMM27 force field[62,63] is employed for the lipids, proteins, and water molecules (TIP3P potential[64]), and the parameters used for the BChla pigments and lycopenes can be found in ref 54. The electrostatic potential is calculated with the Particle Mesh Ewald method, and the bond distances are fixed using the LINCS algorithm.[65] The v-rescale thermostat[66] with a temperature of 310 K was used. When the BChla pigments are in an excited state (population), the surface-hopping method as described in refs 49 and 50 is used to include the change in potential energy of the classical degrees of freedom due to the excitation.

More details of the propagation of the mixed quantum-classical system and the calculation of the linear and 2D spectra using the surface hopping method can be found in refs 49 and 50. Here we give only a brief summary. The time dependence of the state of the quantum subsystem is described by the time-dependent Schrödinger equation, and the equation of motion of the classical degrees of freedom are Newtonian-like. The equations of motion for the quantum and classical subsystem are coupled because the classical degrees of freedom influence the quantum Hamiltonian, and, vice versa, the quantum state influences the forces on the classical atoms. The classical and quantum subsystem are, therefore, numerically integrated in an in-turn fashion. We propagate the quantum subsystem using a scheme based on the Trotter formula[67] using a time step of 1 fs, assuming that the Hamiltonian is constant during this time step. The propagated quantum state is then used to calculate the forces on the classical degrees of freedom, which are then propagated in a single time step using the Velocity Verlet

DOI: 10.1021/jp509247p
J. Phys. Chem. B 2015, 119, 1302−1313

method,[61,68] after which the quantum state is propagated again. The spectra are obtained by summing over the different Liouville pathways contributing to the linear response and third-order response, for the linear spectra and 2D spectra, respectively. A Fourier transform is performed over the coherence times to obtain spectra in the frequency domain.[69,70] For the linear response functions the system is initially excited by a laser pulse at a time τ_1, after which a signal is emitted at a time τ_2. During the time interval $t_1 = \tau_2 - \tau_1$ the system is in a coherence between a single excited state and the ground state. The linear spectrum is obtained by Fourier transforming the temporal two-point correlation function of the transition dipoles over the coherence time t_1

$$S_A(\omega) = \mathrm{Im}\left[\int_0^{t_1^{\max}} \frac{i}{\hbar}\langle \mu^{01}(\tau_2)\mathbf{U}^{11}(\tau_2, \tau_1)\mu^{10}(\tau_1)\rangle_E e^{-i\omega t_1}\, dt_1\right] \quad (4)$$

where $\mathbf{U}^{11}$ denotes the time propagator of the quantum system in the single excitation manifold. In principle, the coherence between the single excited state and ground state will influence the dynamics of the classical system and, therefore, the trajectory of the quantum Hamiltonian. For the surface-hopping method the quantum feedback on the classical degrees of freedom is determined by the so-called "auxiliary" wave function, which, in our case, is always an eigenstate of the Hamiltonian.[48] During the time t_1 the quantum system is in a coherence between excitation manifolds, however, and it is unclear how to calculate the quantum feedback using the surface-hopping method. Recently, a surface-hopping approach was developed for the propagation of such quantum coherences and applied for the calculation of linear spectra.[71] Because of dephasing effects, however, the quantum feedback during the times t_1 hardly affect the response functions[49] and, therefore, are neglected in the current study.

For the third-order response there are three interactions with the laser pulses at times τ_1, τ_2, and τ_3, after which a signal is emitted by the system at a time τ_4. The third-order response function can be split into six different Liouville pathways contributing to the signal. These are the rephasing and nonrephasing parts of the groundstate bleach (GB), stimulated emission (SE), and excited-state absorption (EA) diagrams.[69,70] During the time between the first and second laser pulse $t_1 = \tau_2 - \tau_1$ the system is in a coherence between the ground and excited state for all diagrams. During the waiting time between the second and third laser pulse $t_2 = \tau_3 - \tau_2$ the system is in the ground state for the GB diagrams, whereas it is in a coherence between two single excited states or a population for the SE and EA diagrams. During $t_3 = \tau_4 - \tau_3$ the GB and SE diagrams are both in a coherence between the ground and excited states. For the EA diagrams the system is in a coherence between the double excited state (two electronic excitations) and a single excited state. The 2D spectra for a fixed waiting time t_2 is obtained by adding the responses of the individual diagrams and double Fourier transforming over the coherence times t_1 and t_3. The state of the quantum state is different for the individual diagrams. Therefore, the classical trajectory due to the quantum feedback will also be different. We neglect the quantum feedback when the quantum system is in a coherence because the effects on the 2D spectra are slow compared with the dephasing times.[49,72] We include the quantum feedback for the propagation of the populations during the waiting time t_2, which dominate the third-order response functions, especially for longer waiting times.[49,72]

The spectra are averaged over multiple starting configurations of the simulation box, which are extracted from a ground-state molecular dynamics trajectory, separated by 1 ps. We average the (non)linear spectra over the orientational coefficients for an isotropic sample to include the polarization dependence of the laser pulses in the laboratory frame on the optical response.[70,73] Finally, the third-order response functions are multiplied with a windowing function of the form

$$\mathcal{R}(t_1, t_2, t_3) = \mathcal{R}(t_1, t_2, t_3) 0.5^{(t_1+t_3)^2/T^2} \quad (5)$$

to smoothen the 2D-spectra, where $T = 0.3$ ps is used.

RESULTS

Site Energies, Couplings, and Correlations. In Figure 2 the site energy distributions of the chromophores and the averages of the most important couplings are shown for a trajectory of 2.25 ns for which the Hamiltonian was calculated at every time step of 1 fs. We fitted these distribution functions to a Gaussian function, and the parameters for the fit are given in Table 1. The pigments forming the B850 ring (labeled BChla α and BChla β) and the B800 pigments (labeled BChla γ) have different average transition frequencies. These differences in frequency shifts arise from the different electrostatic interaction with the local environment of the chromophores. The transition energies of the BChla α and BChla β chromophores forming the B850 ring are on average splitted by 80 cm^{-1}, which is due to their different positions with respect to the protein scaffold. The size of their fluctuations is identical, however. The B800 pigments on average have a higher transition frequency of 360 cm^{-1} than the B850 chromophores. This splitting mainly results due to their different binding pockets, which for the B800 pigments are hydrophilic whereas they are hydrophobic for the B850 pigments.[6,25] The distribution of the B800 pigments is about twice as broad, which is attributed to the more polar environment surrounding the B800 ring.[38]

The site energy distributions calculated by Olbrich et al.[38] using semiempirical electronic structure calculations with an identical simulation box result in a much smaller splitting between the B800 and B850 pigments of ∼40 cm^{-1} only. For the calculation of the linear spectra, Olbrich et al. shifted the B800 pigment frequencies by an additional 355 cm^{-1}, however, to match the observed splitting between the two bands. In ref 25 the charge density coupling method was applied to a static LH2 setup using the structural data in the Protein Data Bank (1NKZ[74]), where the lipids and solution are absent. This yielded a splitting between the site energies of the B800 and B850 pigments in the range 234−334 cm^{-1}, depending on the protonation state, which is similar to the 360 cm^{-1} obtained by us. The method of ref 25 gave a splitting between the BChla α and β pigments in the range 360−372 cm^{-1}, which is much larger than the 80 cm^{-1} obtained here. This discrepancy might result from the electrostatic interaction of the pigments with the lipids that surround the protein scaffold and BChla rings, which are included in the present study but are absent in the PDB file. However, in the fitting/modeling of circular dichroism spectra a splitting between the BChla α and β pigments of ∼300 cm^{-1} has previously been assumed,[75,76] which is larger than the splitting we obtain based on the structural information.

DOI: 10.1021/jp509247p
J. Phys. Chem. B 2015, 119, 1302−1313

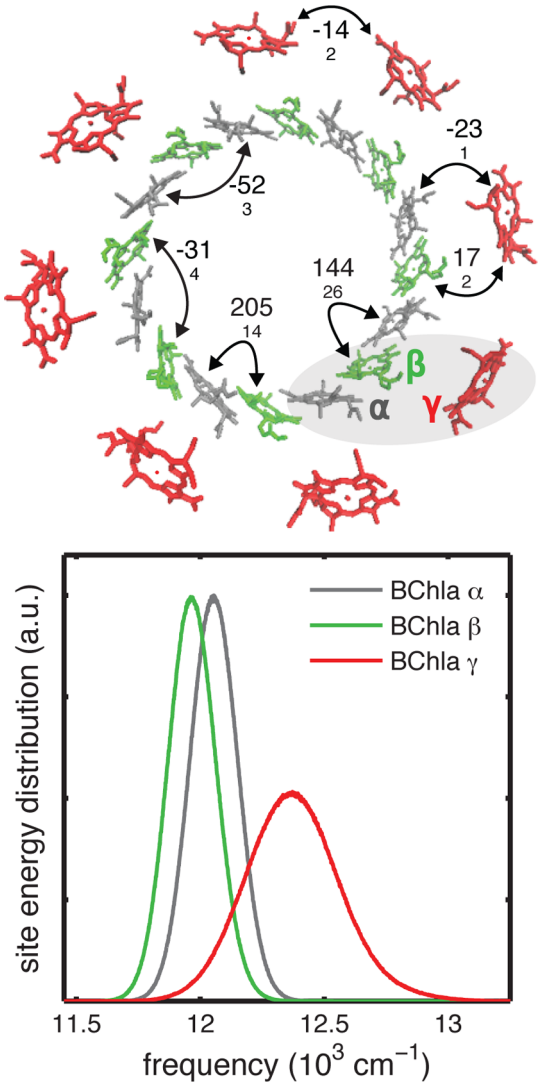

Figure 2. Top: Schematic overview of the LH2 complex. The chromophores of a single trimer unit are labeled as α, β, and γ. The average coupling constants of the strongest interactions between the chromophores are given (large font) and their standard deviations (small font) in wave numbers. The couplings are averaged over a 2.25 ns trajectory and over identical pairs due to the eight-fold symmetry of the system. Bottom: Site energy distributions for the BChla chromophores (α, β, and γ) of the LH2 for the same trajectory. The distributions have been averaged over by symmetry identical chromophores.

Table 1. Fit Parameters for Gaussian Functions Perfectly Matching the Chromophores Site Energy Distributions in Figure 2

BChla	$\bar{\omega}$ (cm^{-1})	σ (cm^{-1})
α	12 050	135
β	11 970	135
γ	12 370	265

The chromophores in the B850 ring are closely packed and, therefore, are strongly coupled. The B850 pigments form a dimerized aggregate, where the nearest neighbor distance between BChla α and BChla β pigments within a single dimer unit is smaller than the distance between chromophores of adjacent dimer units. Because of these distance differences and the relative orientation of the transition dipoles, the nearest average neighbor coupling between pigments within such a dimer unit (215 cm^{-1}) is stronger than the average coupling between nearest neighbor pigments of adjacent dimers (150 cm^{-1}). The average couplings between nearest B800 pigments are much weaker (14 cm^{-1}) due to their larger separation. The strongest couplings between the B800 and B850 ring are 17 and −23 cm^{-1} between the B800 pigments and nearest BChla α/BChla β pigments, respectively. These couplings are weak due to the separation between the pigments as well as the relative orientation between the B800 pigments and the B850 pigments. From spectroscopic studies the strongest couplings within the B850 ring are estimated to be around 250−300 cm^{-1}, which is slightly higher than the couplings we obtain. The strength of the obtained couplings within the used coupling map is proportional to the square of the rescaling factor used for the transition charges, which we optimized to obtain the right peak−peak separation in the linear spectra. The width of the distributions of the couplings is small, as indicated by the standard deviations in Figure 2. The fluctuations of the couplings arise due to the slight variation of the distances between chromophores. Furthermore, the transition dipoles of the chromophores vary in direction and strength due to the movement of individual units that form the chromophores, with respect to each other. The distributions of the transition dipole strengths of the chromophores are shown in Figure 3.

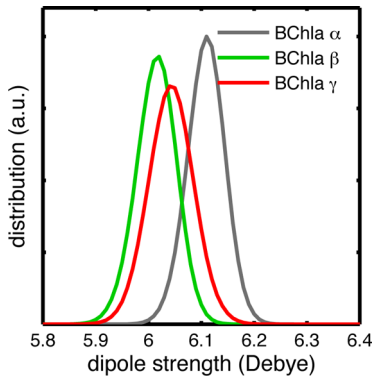

Figure 3. Distributions of the transition dipole strengths of the BChla α, β, and γ pigments for a trajectory of 2.25 ns.

For LH2 beating signals have been observed in the 2D spectra, which have been interpreted as long-lived electronic coherences.[16] The chromophores in the LH2 complex are closely packed and share a similar environment, which might cause a strong correlation between the fluctuations of their transition frequencies. Such a correlation can enhance energy transfer and has been used to explain the long-lived coherences observed in photosynthetic systems.[21,77] To see whether the site energy fluctuations are correlated for LH2 and thereby preserve electronic coherences, we calculate the spatial cross correlation functions between the site energies of the pigments defined as

$$C_{ij} = \frac{1}{\sqrt{\sigma_i^2 \sigma_j^2}} \langle (\omega_i - \bar{\omega}_i)(\omega_j - \bar{\omega}_j) \rangle \tag{6}$$

Here $\langle ... \rangle$ denotes the average over the trajectory, $\bar{\omega}_i$ is the average transition frequency of chromophore i, and σ_i is the standard deviation of the fluctuations. In Figure 4 the cross-correlation coefficients are shown for all pairs of the 24

DOI: 10.1021/jp509247p
J. Phys. Chem. B 2015, 119, 1302−1313

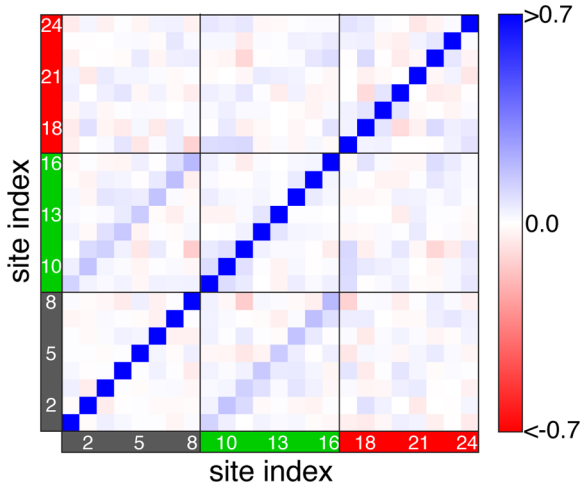

Figure 4. Spatial cross correlation functions between site frequencies of the 24 pigments averaged over a trajectory of 2.25 ns. The site indexes 1−8, 9−16, and 17−24 indicate the BChla α, β, and γ pigments, respectively.

pigments. On the diagonal the correlation is by definition equal to unity. We find a small correlation between the site energies of nearest neighbor BChla α and BChla β pigments within the dimer units in the B850 ring. The correlation coefficient averaged over the eight by symmetry identical pairs (within the dimer units) is 0.17 with a standard deviation of 0.07. Other correlations coefficients are even smaller and negligible compared with the remaining noise. We, therefore, conclude that cross correlations are insignificant for the LH2 complex. This agrees with what was previously reported by Olbrich et al.,[38] although there, a much shorter trajectory of 12 ps was used. For this short trajectory it is hard to distinguish the correlation coefficients from the noise, which is evident from the different correlation coefficients found in ref 38 for the by symmetry identical pairs.

Linear Spectra and Eigenstate Analysis. In Figure 5 the simulated linear spectrum is shown together with the measured

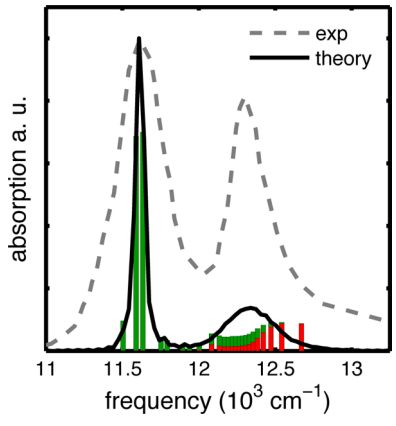

Figure 5. Observed (dashed line) and calculated (solid line) absorption spectra for LH2. The calculated spectra are sampled over 1500 different starting configurations, extracted from a ground-state trajectory of 1.5 ns. The bars indicate the average energy of the eigenstates, and the height indicates their average transition dipole strengths squared. The green and red colors of the bars show the participation of inner and outer ring chromophores to the eigenstate, respectively.

spectrum[7] The average energies of the eigenstates are indicated by the bars whose heights correspond to the absorption cross section of the states. The coherence time t_1 is included in the range of 0 until 0.5 ps to obtain the first-order response functions. The response functions are, furthermore, averaged over 1500 starting configurations of the simulation box. The simulated absorption spectrum reproduces the observed two-peak structure, and the splitting between the two bands indeed matches the experimental data. The low-energy band results from the absorption of multiple states but the main contribution comes from two nearly degenerate superradiant states, also known as the $k = \pm 1$ states.[8] The lowest energy $k = 0$ eigenstate has a significant transition dipole moment and recently has been observed in single-molecule fluorescence spectra.[78] According to our simulations it is red-shifted from the $k \pm 1$ states by ∼110 cm^{-1}. For a circular structure without disorder the transition dipole moment of the $k = 0$ is expected to be small because it results only from the out-of-plane components of the transition dipoles of the pigments. Because of the disorder in the system, however, the $k = 0$ state gains significant oscillator strength from nearby states.[9] The states within the low-energy band are all completely localized on the B850 ring and therefore also referred to as the B850 states. The lower energy part of the high-energy band results from the absorption of multiple states with rather weak transition dipole moments. These states are delocalized over both the B850 and B800 ring (B850* states). The high-energy absorption within the high-energy band results from the absorption of states mainly localized on the B800 ring (B800 states). A measure for the spatial delocalization of these excitonic eigenstates is the coherence length. Several definitions exist for the coherence length,[79,80] and we use the following[81,82]

$$L_\rho = \frac{(\sum_{ij}^{N} |\rho_{ij}|)^2}{N \sum_{ij}^{N} |\rho_{ij}|^2} \tag{7}$$

where ρ is the density matrix corresponding to an eigenstate in the site basis and N is the number of chromophores. For a perfectly coherent state all elements of the density matrix have an absolute value equal to $1/N$, leading to a coherence length of $L_\rho = N$. When a state is localized on a single pigment, however, only the single diagonal element of the density matrix corresponding to that site has nonzero value of 1, leading to a coherence length of $L_\rho = 1/N$. We plotted the coherence length obtained for the 24 eigenstates in the first excitation manifold in Figure 6, averaged over a ground-state trajectory of 2.25 ns. The states in the low-energy band are highly delocalized over about half the inner ring. In refs 33 and 80 similar coherence lengths where obtained in model studies of LH2. Such a strong delocalization of the states in a way enhances the energy transfer in the system because these states make the complex robust against the trapping of an excitation. The B850* states are slightly delocalized over a couple of B800 and B850 pigments. The high-frequency B800 states are essentially localized at single outer ring chromophores.

The simulated result for the absorption spectrum has a low-energy band that is much narrower than the one observed in the experiment. The experimental spectra are measured for an ensemble of LH2 complexes, whereas in the simulations only a single LH2 complex is considered. Within the 2.25 ns trajectory we are able to catch the fast nuclear fluctuations but not the slow structural changes of the complex (static disorder). Furthermore, the C8 symmetry structure of the LH2 complex

DOI: 10.1021/jp509247p
J. Phys. Chem. B 2015, 119, 1302−1313

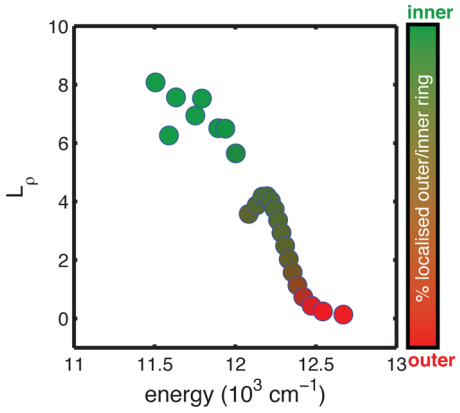

Figure 6. Coherence length for the eigenstates in the first excited-state manifold as a function of their energy. The coherence lengths are averaged over a trajectory of 2.25 ns for which the Hamiltonian was calculated at every time step of 1 fs. The colors indicate how much the eigenstate is localized on the inner ring (green color) and outer ring (red color) averaged over the whole trajectory.

within our simulation is based on X-ray crystallography experiments where the LH2 complexes are extremely densely packed. This C8 symmetry leads to nearly degenerate $k = \pm 1$ states, regardless of diagonal disorder. From low-temperature fluorescence spectroscopy measurements on single LH2 complexes, a large splitting between the two superradiant states is, however, observed.[8] This splitting can be explained only by a structural deformation (disorder in the couplings) of the protein complex, like a two-fold symmetrical elliptical structure.[8,28,83] The structure of the LH2 complexes thus depends on the environment surrounding the LH2 complexes (density of the samples), and it cannot be excluded that the structure of LH2 in purple bacteria differs from the one in crystals.

Static disorder in the transition frequencies[28,84,85] and in the couplings[8,9,75,86,87] have been commonly added to theoretically describe/fit different experimental observables for LH2. The B850 band is narrow in our simulations due to exchange narrowing and therefore is rather insensitive to diagonal disorder. The band, however, is sensitive to correlated off-diagonal disorder. Within the ensemble it is possible that LH2 complexes with different geometries exist like, for example, stretched or elliptically deformed rings. Such deformations result in off-diagonal disorder that can broaden the B850 band.[8,9,86] Within our simulation box only a single circular LH2 complex is present. We choose to maintain its circular structure (C8 symmetry), based on the X-ray data, however, but include static off-diagonal disorder in the following ad hoc way. Instead of using a constant rescaling factor of 0.7 for the transition charges for calculating the couplings (eq 3), the rescaling factor for a single sample is determined by drawing a random number from a normal distribution with a mean of 0.7 and a standard deviation of 0.15. The C8 symmetry of the complex is maintained in this way because all couplings within a single sample are rescaled with the same factor. We, therefore, effectively sample over LH2 complexes with different radii, like was done in ref 87. Within the simulation there are five POPC lipids surrounded by the protein scaffold. One could imagine that one more-or-less POPC lipid could slightly change the radius of the pigment−protein complex, which changes the distance between the pigments and thereby the couplings.

The simulated linear spectrum including the off-diagonal disorder is shown in Figure 7. The B850 band has become much broader than before and matches the experimental data much better. A sample with a larger rescaling factor gives rise to a narrow B850 band at a lower energy than a sample with a smaller rescaling factor. It is the average of all of the separate contributions of the different samples that leads to the broadening of the B850 band. The B800 band is hardly affected by the rescaling due to the localized nature of the excitations. Although the inclusion of static off-diagonal disorder gives rise to a significant improvement of the linear spectrum, the widths of the bands and their relative intensities still do not perfectly match the experiment. The simulations strongly depend on the mappings used for the transition frequencies, couplings, and transition dipoles. Moreover, the force field used to describe the atomistic environment determines the positions of the atoms in the simulation box and, therefore, all of the above quantities. Optimizations of the mappings and force fields will lead to improved simulated spectra. Here we used the approximate charge density coupling method to determine the transition frequencies, which is computationally cheap compared with semiempirical structure calculations. This allows for rather long trajectories needed for the calculation of 2D spectra. Furthermore, the utilization of such a mapping allows for the computation of the derivatives of the excited-state potential, which are needed to determine the influence of the quantum state on the environment.

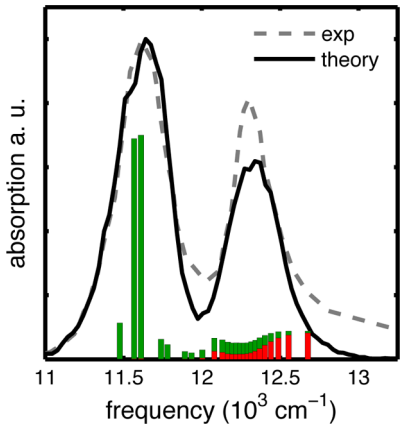

Figure 7. Observed (dashed line) and calculated (solid line) absorption spectra for LH2. The calculated spectrum is sampled over 1500 starting configurations including static off-diagonal disorder for the couplings. The bars indicate the average energy of the eigenstates, and the height indicates their average absorption intensity. The green and red colors of the bars show how much on average the state is localized on the inner and outer rings, respectively.

2D Spectra and Energy Transfer. In Figure 8 the simulated all-parallel polarization 2D spectra are shown for a waiting time of $t_2 = 0$ and 250 fs. The 2D spectra are depicted for calculations where the feedback is included using the surface-hopping method (left) and, for comparison, calculations where the feedback is neglected (NISE method[72,88]). The simulations included the static off-diagonal disorder as discussed for the linear absorption. The coherence times t_1 and t_3 were varied from 0 until 0.2 ps. The zero waiting time 2D spectra for the surface hopping and NISE method are identical and show two diagonal peaks corresponding to the B850 and B800 bands. The B850 band has much more intensity than the

DOI: 10.1021/jp509247p
J. Phys. Chem. B 2015, 119, 1302−1313

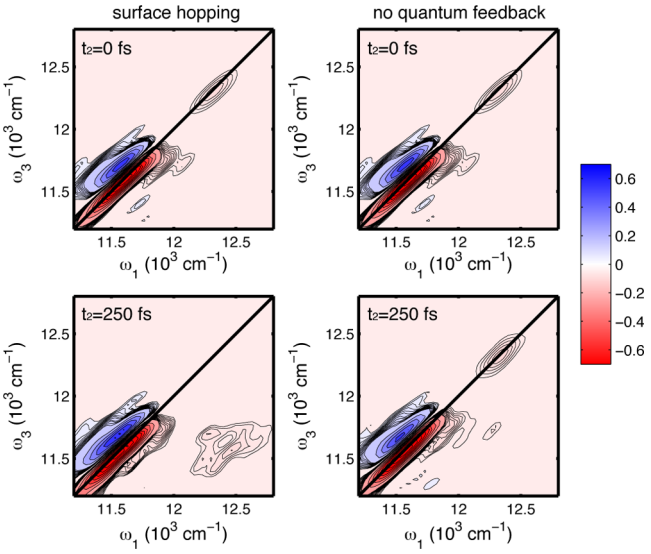

Figure 8. All-parallel polarization 2D spectra of the LH2 complex for two different waiting times of 0 (top) and 250 fs (bottom) simulated using the surface hopping method (left) and calculations where the quantum feedback is neglected (right). The spectra for t_2 = 0 and 250 fs have been sampled over 1500 and 150 initial configurations of the simulation box, respectively.

B800 band. It was shown above that the B850 band mainly results from the absorption of two superradiant states with strong transition dipole moments, whereas the B800 band results from the absorption of many states with rather weak transition dipoles. Because the 2D spectra depend on the transition dipole to the fourth power, the B850 band is much more pronounced than the B800 band. The negative-valued peaks along the diagonal in the 2D spectra result from the stimulated emission and ground-state bleach contributions. At the low-energy band there is a high-intensity positive peak above the diagonal resulting from the excited-state absorption. The splitting between these two peaks is ∼150 cm^{-1} and the excited-state absorption peak has 64% of the intensity of the ground-state bleach/stimulated emission peak. A similar peak structure has been observed in 2D-spectra of J-aggregates, and this feature is a typical indication of a strong delocalization of the states.[89,90] For the B800 band such a positive peak is not visible in the 2D-spectra because the molecules are weakly coupled, leading to states that are localized on a few molecules. Therefore, the excited-state absorption contributions are canceled by the stimulated emission and ground-state bleach signals. The 2D spectra measured for short waiting times in ref 17 for an LH2 complex of the species *Rhodobacter sphaeroides* (nine-fold symmetry) show qualitatively similar peak structures; however, a direct comparison is not suitable. This is because of the difference in bacterial species and the narrow pulse shape employed in the experiment, which was not included in the simulations.

The 2D spectra for a waiting time of 250 fs in Figure 8 are very different for the calculations including and excluding the quantum feedback. The spectrum calculated using the surface hopping method shows the growth of a substantial cross-peak below the diagonal indicating energy transfer from the B800 band to the B850 band, whereas for the NISE method the intensity of this cross-peak is much weaker. The diagonal B800 peak is no longer visible for the surface-hopping method due to the B800 → B850 relaxation and the weak transition dipole moments of the states in the B800 band. The significant differences in cross-peak growth for the two methods arise from the fact that neglecting the quantum feedback is an infinite temperature approximation.[72,88] Upon initial excitation of the B800 band, most of the excitation will relax toward the low-energy states when the waiting time is increased for surface-hopping method, due to detailed balance. This leads to the considerable growth of the lower cross-peak. For the NISE method, however, the equilibrium situation is independent of the temperature and the excitation is spread equally over all states. Therefore, most of the population will recite in the high-energy band (16 states) when the waiting time is increased and contribute to the B800 diagonal peak in the 2D spectra, instead of relaxing to the low-energy band (8 states). To describe the population transfer within the system properly and, thereby, the growth of the cross-peaks, it is essential that the quantum feedback is included.

The measured 2D-spectra by Fidler et al.[17] show the growth of a significant cross-peak on a hundreds of femtosecond time scale as well. Furthermore, the low-energy band in the measured spectra for nonzero waiting times exhibits a Stokes shift of about 110 cm^{-1}.[17] This Stokes shift can arise from the strong interaction between the quantum excitation and the bath, which can cause a dynamic localization of the excitation.[18,91−93] Such a Stokes shift and exciton localization is, however, not observed in our simulations where the reorganization of the environment due to the excitation is included using the surface hopping method.[48−50] Since the states within the B850 band are delocalized over multiple chromophores, the additional forces are spread out over a large area and the reorganization of the environment, therefore, is small. On the basis of this observation, we think that the experimental Stokes shift results from intraband relaxation within the B850 band instead. According to fluorescence experiments on LH2 the energy splitting between the two superradiant states within the B850 band is ∼110 cm^{-1},[8] which is similar to the observed Stokes shift. Although relaxation of the excitation is included in our simulations, such a splitting between the $k \pm 1$ states is absent due to the inherent C8 symmetry of the LH2 complex crystal structure, as was previously described. Furthermore, the simulations presented here neglect the intramolecular vibrations of the pigments, which can affect the excited-state dynamics and can cause a peak shifted from the diagonal in the 2D spectra as well. Recently, the influence of such vibronic couplings on the electronic coherences measured in the 2D spectra has been studied extensively,[23,60] although it has been demonstrated that the contribution of intramolecular vibrations to the spectral density is negligible for BChla.[59] Their inclusion in our atomistic simulations, interesting as it may be, at this moment is computationally too costly.

To study the energy transfer from the high-energy band to the low-energy band in a more elaborate way we calculate the population transfer diagrams depicted in Figure 9. The 24 eigenstates in the first excitation manifold are labeled 1−24 (from low to high energies) and are divided into three groups. The eight eigenstates lowest in energy form the B850 band and are labeled as the B850 states. The eigenstates 9−16 absorb in the low-energy part of the B800 band but are strongly localized on the inner (B850) ring and therefore are labeled as the B850* states. The eight eigenstates highest in energy are labeled as the B800 states. Initially the highest energy eigenstate (24) was excited and the probability for finding the excitation in

DOI: 10.1021/jp509247p
J. Phys. Chem. B 2015, 119, 1302−1313

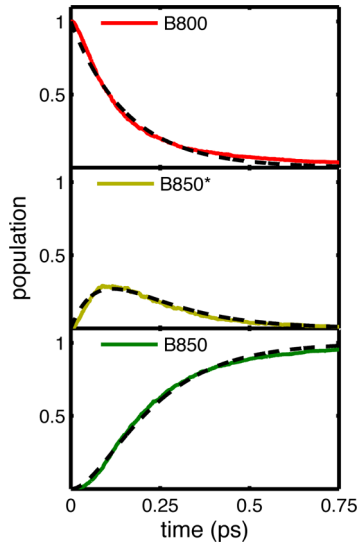

Figure 9. Average population of the B850 (bottom), B850* (middle), and B800 (top) states as a function of time after initial excitation of the highest energy eigenstate in the first excitation manifold calculated using the surface-hopping method. The data is averaged over 1500 starting configurations of the simulation box. The dashed lines indicate the fits of the data to a kinetic model.

each subset of eigenstates is shown as a function of time in Figure 9 for the surface-hopping method. The excitation first relaxes within the B800 band from the B800 states to the lower energy B850* states. The excitation is then already partially localized on the inner ring and from there can transfer to the B850 band. After a time of 0.75 ps most of the population is in the B850 states., as is expected from detailed balance. The presence of the intermediate B850* states thus allows for a stepwise downhill energy transfer from the B800 band to the B850 band. In refs 34 and 35 Redfield theory was applied to an LH2 complex at a temperature of 77 K, and a similar relaxation pathway was found albeit with slower relaxation times due to the lower temperature.[94]

To extract the time scales for the intraband B800 → B850* and the interband B850* → B850 energy transfer calculated using the surface-hopping method we fitted the population transfer data to the following simple kinetic model

$$\frac{dN_{800}(t)}{dt} = -\lambda_1 N_{800}(t)$$
$$\frac{dN_{850^*(t)}}{dt} = -\lambda_2 N_{850^*}(t) + \lambda_1 N_{800}(t)$$
$$\frac{dN_{850(t)}}{dt} = \lambda_2 N_{850^*}(t) \quad (8)$$

excluding direct relaxation from the B800 states to the B850 states. The dashed lines in Figure 9 show the results of the kinetic model fit, which almost perfectly correspond to the original data. The obtained time scales for the relaxation constants are λ_1 = 6.35 1/ps and λ_2 = 11.18 1/ps. Within our simulations the relaxation process from the B800 band to the B850 band is completed after 0.75 ps. This corresponds to the observed interband relaxation time scale of 0.7 ps observed in transient absorption experiments on the LH2 complex of *Rhodobacter sphaeroides*.[94,95] From the growth of the B800 → B850 cross peak in the 2D-spectra of the LH2 complex of *Rhodobacter sphaeroides* a time scale of 0.7 ps was determined as well. Furthermore, the 2D spectra were reported to be indistinguishable for waiting times from 1 ps onward, indicating the system has completely relaxed in the first excitation manifold within 1 ps, which is similar to our observations.

CONCLUSIONS

We calculated (non)linear spectra of LH2 using mixed quantum-classical simulations and studied energy transport within the complex using the surface-hopping method. The simulation method includes the interaction of the chromophores and their environment in an atomistic way using molecular dynamics simulations and therefore provides detailed information on the influence of the surroundings on the transition frequencies, transition dipoles, and energy transport in the system. For a ground-state molecular dynamics trajectory we showed that the chromophores positions and binding pockets strongly influence their average transition frequencies and the size of the fluctuations. Although the chromophores are closely packed, we showed that the site energies of neighboring pigments are practically uncorrelated and therefore conclude that such correlations cannot be used to explain the long-lived beating signals observed in the 2D spectra.[16]

We simulated the linear absorption spectra for the LH2 complex and were able to reproduce the two-band structure. Additional off-diagonal disorder by averaging over LH2 complexes with different radii was added to broaden the B850 band, resulting in a good match in the peak distance and peak width. We showed that this low-energy band results from the absorption of states that are highly delocalized over multiple B850 pigments. Because of the strong coupling in the B850 ring, the inner ring pigments, however, also contribute to the high-energy band. These B850* states have nonzero transition dipole moments and are delocalized over multiple B850 and B800 pigments. Furthermore, we showed that the high-energy part of the B800 band mainly results from the absorption of single B800 pigments.

Finally, we presented the first atomistic mixed quantum-classical simulations of 2D-spectra for the LH2 complex. The simulations show qualitatively agreement with experimental data on LH2 complexes of the species *Rhodospirillum acidophila* with a nine-fold symmetry.[17] The substantial growth of a cross peak on a time scale of hundreds of femtoseconds below the diagonal indicates rapid energy transfer from the B800 band to the B850 band. We showed that the nature of the states in the complex allows for a stepwise downhill energy transfer. Upon excitation of the B800 states, first an intraband relaxation occurs to the B850* states, after which the excitation can transfer to the low-energy band.

AUTHOR INFORMATION

Corresponding Author

*E-mail: t.l.c.jansen@rug.nl.

Notes

The authors declare no competing financial interest.

ACKNOWLEDGMENTS

This work is part of the research programme of the Foundation for Fundamental Research on Matter (FOM), which is part of The Netherlands Organization for Scientific Research (NWO). U.K. thanks the Deutsche Forschungsgemeinschaft (DFG) for support through grant No. KL 1299/12-1.

DOI: 10.1021/jp509247p
J. Phys. Chem. B 2015, 119, 1302−1313

REFERENCES

(1) Amerongen, H. v.; Valkunas, L.; Grondelle, R. v. *Photosynthetic Excitons*; World Scientific: River Edge, NJ, 2000.

(2) Miller, K. Three-Dimensional Structure of a Photosynthetic Membrane. *Nature* **1982**, *300*, 53−55.

(3) Hu, X.; Ritz, T.; Damjanović, A.; Autenrieth, F.; Schulten, K. Photosynthetic Apparatus of Purple Bacteria. *Q. Rev. Biophys.* **2002**, *35*, 1−62.

(4) McDermott, G.; Prince, S. M.; Freer, A.; Hawthornthwaite-Lawless, A. M.; Papiz, M. Z.; Cogdell, R. J.; Isaacs, N. W. Crystal Structure of an Integral Membrane Light-Harvesting Complex from Photosynthetic Bacteria. *Nature* **1995**, *374*, 517−521.

(5) Cogdell, R. J.; Isaacs, N. W.; Freer, A. A.; Howard, T. D.; Gardiner, A. T.; Prince, S. M.; Papiz, M. Z. The Structural Basis of Light-Harvesting in Purple Bacteria. *FEBS Lett.* **2003**, *555*, 35−39.

(6) Koepke, J.; Hu, X.; Muenke, C.; Schulten, K.; Michel, H. The Crystal Structure of the Light-Harvesting Complex II (B800−850) from Rhodospirillum Molischianum. *Structure* **1996**, *4*, 581−597.

(7) Zhang, J.-P.; Fujii, R.; Qian, P.; Inaba, T.; Mizoguchi, T.; Koyama, Y. Mechanism of the Carotenoid-to-Bacteriochlorophyll Energy Transfer via the S1 State in the LH2 Complexes from Purple Bacteria. *J. Phys. Chem. B* **2000**, *104*, 3683−3691.

(8) van Oijen, A. M.; Ketelaars, M.; Köhler, J.; Aartsma, T. J.; Schmidt, J. Unraveling the Electronic Structure of Individual Photosynthetic Pigment-Protein Complexes. *Science* **1999**, *285*, 400−402.

(9) Ketelaars, M.; van Oijen, A. M.; Matsushita, M.; Köhler, J.; Schmidt, J.; Aartsma, T. J. Spectroscopy on the B850 Band of Individual Light-Harvesting 2 Complexes of Rhodopseudomonas Acidophila I. Experiments and Monte Carlo Simulations. *Biophys. J.* **2001**, *80*, 1591−1603.

(10) Oellerich, S.; Köhler, J. Low-Temperature Single-Molecule Spectroscopy on Photosynthetic Pigment-Protein Complexes from Purple Bacteria. *Photosynth. Res.* **2009**, *101*, 171−179.

(11) Cogdell, R. J.; Köhler, J. Use of Single-Molecule Spectroscopy to Tackle Fundamental Problems in BioChemistry: Using Studies on Purple Bacterial Antenna Complexes as an Example. *Biochem. J.* **2009**, *422*, 193−205.

(12) Kunz, R.; Timpmann, K.; Southall, J.; Cogdell, R.; Freiberg, A.; Köhler, J. Exciton Self Trapping in Photosynthetic Pigment-Protein Complexes Studied by Single-Molecule Spectroscopy. *J. Phys. Chem. B* **2012**, *116*, 11017−11023.

(13) Kunz, R.; Timpmann, K.; Southall, J.; Cogdell, R.; Freiberg, A.; Köhler, J. Fluctuations in the Electron-Phonon Coupling of a Single Chromoprotein. *Angew. Chem., Int. Ed.* **2013**, *52*, 8726−8730.

(14) Hybl, J. D.; Albrecht, A. W.; Gallagher Faeder, S. M.; Jonas, D. M. Two-Dimensional Electronic Spectroscopy. *Chem. Phys. Lett.* **1998**, *297*, 307−313.

(15) Brixner, T.; Stenger, J.; Vaswani, H. M.; Cho, M.; Blankenship, R. E.; Fleming, G. R. Two-Dimensional Spectroscopy of Electronic Couplings in Photosynthesis. *Nature* **2005**, *434*, 625.

(16) Harel, E.; Engel, G. S. Quantum Coherence Reveals Complex Dynamics in Bacterial Light-Harvesting Complex 2 (LH2). *Proc. Natl. Acad. Sci. U.S.A.* **2012**, *109*, 706−711.

(17) Fidler, A. F.; Singh, V. P.; Long, P. D.; Dahlberg, P. D.; Engel, G. S. Probing Energy Transfer Events in the Light Harvesting Complex 2 (LH2) of Rhodobacter Sphaeroides with Two-Dimensional Spectroscopy. *J. Chem. Phys.* **2013**, *139*, 155101.

(18) Filder, A. F.; Singh, V. P.; Long, P. D.; Dahlberg, P. D.; Engel, G. S. Dynamic Localization of Electronic Excitation in Photosynthetic Complexes Revealed with Chiral Two-Dimensional Spectroscopy. *Nat. Commun.* **2014**, *5*, 3286.

(19) Cho, M. *Two-Dimensional Optical Spectroscopy*; CRC Press: Boca Raton, FL, 2009.

(20) Collini, E.; Wong, C. Y.; Wilk, K. E.; Curmi, P. M. G.; Brumer, P.; Scholes, G. D. Coherently Wired Light-Harvesting in Photosynthetic Marine Algae at Ambiant Temperature. *Nature* **2010**, *463*, 644.

(21) Engel, G. S.; Calhoun, T. R.; Read, E. L.; Ahn, T. K.; Mancal, T.; Cheng, Y. C.; Blankenship, R. E.; Fleming, G. R. Evidence for Wavelike Energy Transfer Through Quantum Coherence in Photosynthetic Systems. *Nature* **2007**, *446*, 782.

(22) Panitchayangkoon, G.; Hayes, D.; Fransted, K. A.; Caram, J. R.; Harel, E.; Wen, J. Z.; Blankenship, R. E.; Engel, G. S. Long-Lived Quantum Coherence in Photosynthetic Complexes at Physiological Temperature. *Proc. Natl. Acad. Sci. U.S.A.* **2010**, *107*, 12766−12770.

(23) Christensson, N.; Kauffmann, H. F.; Pullerits, T.; Mančal, T. Origin of Long-Lived Coherences in Light-Harvesting Complexes. *J. Phys. Chem. B* **2012**, *116*, 7449−7454.

(24) Chin, A. W.; Prior, J.; Rosenbach, R.; Caycedo-Soler, F.; Huelga, S. F.; Plenio, M. B. The Role of Non-Equilibrium Vibrational Structures in Electronic Coherence and Re-coherence in Pigment-Protein Complexes. *Nat. Phys.* **2013**, *9*, 113−118.

(25) Rancova, O.; Sulskus, J.; Abramavicius, D. Insight into the Structure of Photosynthetic LH2 Aggregate from Spectroscopy Simulations. *J. Phys. Chem. B* **2012**, *116*, 7803−7814.

(26) Cleary, L.; Cao, J. Optimal Thermal Bath for Robust Excitation Energy Transfer in Disordered Light-Harvesting Complex 2 of Purple Bacteria. *New J. Phys.* **2013**, *15*, 125030.

(27) Scholes, G. D.; Fleming, G. R. On the Mechanism of Light Harvesting in Photosynthetic Purple Bacteria: B800 to B850 Energy Transfer. *J. Phys. Chem. B* **2000**, *104*, 1854−1868.

(28) Novoderezhkin, V. I.; D, R.; van Grondelle, R. Dynamics of the Emission Spectrum of a Single LH2 Complex: Interplay of Slow and Fast Nuclear Motions. *Biophys. J.* **2006**, *90*, 2890−2902.

(29) Jang, S.; Newton, M. D.; Silbey, R. J. Multichromophoric Förster Resonance Energy Transfer from B800 to B850 in the Light Harvesting Complex 2: Evidence for Subtle Energetic Optimization by Purple Bacteria. *J. Phys. Chem. B* **2007**, *111*, 6807−6814.

(30) Jang, S.; Newton, M. D.; Silbey, R. J. Multichromophoric Förster Resonance Energy Transfer. *Phys. Rev. Lett.* **2004**, *92*, 218301.

(31) Sumi, H. Theory on Rates of Excitation-Energy Transfer between Molecular Aggregates through Distributed Transition Dipoles with Application to the Antenna System in Bacterial Photosynthesis. *J. Phys. Chem. B* **1999**, *103*, 252−260.

(32) Bruggemann, B.; May, V. Exciton Exciton Annihilation Dynamics in Chromophore Complexes. II Intensity Dependent Transient Absorption of the LH2 Antenna System. *J. Chem. Phys.* **2004**, *120*, 2325−2336.

(33) Strümpfer, J.; Schulten, K. Light Harvesting Complex II B850 Excitation Dynamics. *J. Chem. Phys.* **2009**, *131*, 225101.

(34) van Grondelle, R.; Novoderezhkin, V. I. Energy Transfer in Photosynthesis: Experimental Insights and Quantitative Models. *Phys. Chem. Chem. Phys.* **2006**, *8*, 793.

(35) Novoderezhkin, V.; Wendling, M.; van Grondelle, R. Intra- and Interband Transfers in the B800-B850 Antenna of *Rhodospirillum Molischianum*: Redfield Theory Modeling of Polarized Pump-Probe Kinetics. *J. Phys. Chem. B* **2003**, *107*, 11534−11548.

(36) Cleary, L.; Chen, H.; Chuang, C.; Silbey, R. J.; Cao, J. Optimal Fold Symmetry of LH2 Rings on a Photosynthetic Membrane. *P. Nat. Acad. Sci.* **2013**, *110*, 8537−8542.

(37) Rancova, O.; Abramavicius, D. On the Static and Dynamic Disorder in Bacterial Light-Harvesting Complex LH2:2DES Simulation Study. *J. Phys. Chem. B* **2014**, DOI: 10.1021/jp5043156.

(38) Olbrich, C.; Kleinekathöfer, U. Time-Dependent Atomistic View on the Electronic Relaxation in Light-Harvesting System II. *J. Phys. Chem. B* **2010**, *114*, 12427−12437.

(39) Olbrich, C.; Jansen, T. L. C.; Liebers, J.; Aghtar, M.; Strümpfer, J.; Schulten, K.; Knoester, J.; Kleinekathöfer, U. From Atomistic Modeling to Excitation Transfer and Two-Dimensional Spectra of the FMO Light-Harvesting Complex. *J. Phys. Chem. B* **2011**, *115*, 8609−8621.

(40) Jing, Y.; Zheng, R.; Li, H. X.; Shi, Q. Theoretical Study of the Electronic-Vibrational Coupling in the Q_y States of the Photosynthetic Reaction Center in Purple Bacteria. *J. Phys. Chem. B* **2011**, *116*, 1164−1171.

DOI: 10.1021/jp509247p
J. Phys. Chem. B 2015, 119, 1302−1313

(41) Zhang, L.; Silva, D. A.; Zhang, H.; Yue, A.; Yan, Y.; Huang, X. Dynamic Protein Conformations Preferentially Drive Energy Transfer Along the Active Chain of the Photosystem II Reaction Centre. *Nat. Commun.* **2014**, *5*.
(42) Valleau, S.; Eisfeld, A.; Aspuru-Guzik, A. On the Alternatives for Bath Correlators and Spectral Densities from Mixed Quantum-Classical Simulations. *J. Chem. Phys.* **2012**, *137*, 224103.
(43) Fujita, T.; Huh, J.; Saikin, S. K.; Brookes, J. C.; Aspuru-Guzik, A. Theoretical Characterization of Excitation Energy Transfer in Chlorosome Light-Harvesting Antennae from Green Sulfur Bacteria. *Photosynth. Res.* **2014**, *120*, 273−289.
(44) Huh, J.; Saikin, S. K.; Brookes, J. C.; Valleau, S.; Fujita, T.; Aspuru-Guzik, A. Atomistic Study of Energy Funneling in the Light-Harvesting Complex of Green Sulfur Bacteria. *J. Am. Chem. Soc.* **2014**, *136*, 2048−2057.
(45) Adolphs, J.; Müh, F.; Madjet, M. E.; Renger, T. Calculation of Pigment Transition Energies in the FMO Protein. *Photosynth. Res.* **2008**, *95*, 197.
(46) Madjet, M. E.; Abdurahman, A.; Renger, T. Intermolecular Coulomb Couplings from Ab Initio Electrostatic Potentials: Application to Optical Transitions of Strongly Coupled Pigments in Photosynthetic Antennae and Reaction Centers. *J. Phys. Chem. B* **2006**, *110*, 17268−17281.
(47) Renger, T.; Madjet, M. E.; Schmidt am Busch, M.; Adolphs, J.; Müh, F. Structure-Based Modeling of Energy Transfer in Photosynthesis. *Photosynth. Res.* **2013**, *116*, 367−388.
(48) HammesSchiffer, S.; Tully, J. C. Proton Transfer in Solution: Molecular Dynamics with Quantum Transitions. *J. Chem. Phys.* **1994**, *101*, 4657.
(49) Tempelaar, R.; Vegte, C. P. v. d.; Knoester, J.; Jansen, T. L. C. Surface Hopping Modeling of Two-Dimensional Spectra. *J. Chem. Phys.* **2013**, *138*, 164106.
(50) van der Vegte, C. P.; Knop, S.; Vöhringer, P.; Jansen, T. L. C.; Knoester, J. OH-Stretching in Synthetic Hydrogen-Bonded Chains. *J. Phys. Chem. B* **2014**, *118*, 6256−6264.
(51) Mukamel, S. Nonimpact unified theory of four-wave mixing and two-photon processes. *Phys. Rev. A* **1983**, *28*, 3480.
(52) Fujita, T.; Huh, J.; Aspuru-Guzik, A. A Stochastic Reorganizational Bath Model For Electronic Energy Transfer. *J. Chem. Phys.* **2014**, *140*, 244103.
(53) Pullerits, T.; Hess, S.; Herek, J. L.; Sundström, V. J. Temperature Dependence of Excitation Transfer in LH2 of Rhodobacter Spaeroides. *J. Phys. Chem. B* **1997**, *101*, 10560−10567.
(54) Damjanović, A.; Kosztin, I.; Kleinekathöfer, U.; Schulten, K. Excitons in a Photosynthetic Light-Harvesting System: A Combined Molecular Dynamics, Quantum Chemistry and Polaron Model Study. *Phys. Rev. E* **2002**, *65*, 031919.
(55) Steffen, M.; Lao, K.; Boxer, S. Dielectric Asymmetry in the Photosynthetic Reaction Center. *Science* **1994**, *264*, 810−816.
(56) Renger, T. Theory of Excitation Energy Transfer: From Structure to Function. *Photosynth. Res.* **2009**, *102*, 471−485.
(57) Renger, T.; Müh, F. Theory of Excitonic Couplings in Dielectric Media: Foundation of Poisson-TrEsp Method and Application to Photosystem I Trimers. *Photosynth. Res.* **2012**, *111*, 47−52.
(58) Hsu, C. P.; Fleming, G. R.; Head-Gordon, M.; Head-Gorden, T. Excitation Energy Transfer in Condensed Media. *J. Chem. Phys.* **2011**, *114*, 3065−3072.
(59) Olbrich, C.; Strümpfer, J.; Schulten, K.; Kleinekathöfer, U. Theory and Simulation of the Environmental Effects on FMO Electronic Transitionsnvironmental Effects on FMO Electronic Transitions. *J. Phys. Chem. Lett.* **2011**, *2*, 1771−1774.
(60) Halpin, A.; Johnson, P. J. M.; Tempelaar, R.; Murphy, R. S.; Knoester, J.; Jansen, T. L. C.; Miller, R. J. D. Two-Dimensional Spectroscopy of a Molecular Dimer Unveils the Effects of Vibronic Coupling on Exciton Coherences. *Nat. Chem.* **2014**, *6*, 196−201.
(61) Spoel, D. v. d.; Lindahl, E.; Hess, A. R.; Buuren, R. v.; Apol, E.; Meulenhoff, P. J.; Tieleman, D. P.; Sijbers, A. L. T. M.; Feenstra, K. A.; Drunen, R. v.; Berendsen, H. J. C. *Gromacs User Manual*, version 4.5.6., 2010.
(62) MacKerell, A. D.; et al. All-Atom Empirical Potential for Molecular Modeling and Dynamics Studies of Proteins. *J. Phys. Chem. B* **1998**, *102*, 3586−3616.
(63) Foloppe, N.; MacKerell, A. D. All-Atom Empirical Force Field for Nucleic Acids: I. Parameter Optimization Based on Small Molecule and Condensed Phase Macromolecular Target Data. *J. Comput. Chem.* **200**, *21*, 86−104.
(64) Jorgensen, W. L.; Chandrasekhar, J.; Madura, J. D.; Impey, R. W.; Klein, M. L. Comparison of Simple Potential Functions for Simulating Liquid Water. *J. Chem. Phys.* **1983**, *79*, 926.
(65) Hess, B.; Bekker, H.; Berendsen, H. J. C.; Fraaije, J. G. E. M. LINCS: A Linear Constraint Solver for Molecular Simulations. *J. Comput. Chem.* **1997**, *18*, 1463.
(66) Bussi, G.; Donadio, D.; Parrinello, M. Canonical Sampling Through Velocity Rescaling. *J. Chem. Phys.* **2007**, *126*, 014101.
(67) Liang, C.; Jansen, T. L. C. An efficient N^3-Scaling Propagation Scheme for Simulating Two-Dimensional Infrared and Visible Spectra. *J. Chem. Theory Comput.* **2012**, *8*, 1706−1713.
(68) Swope, W. C.; Andersen, H. C.; Berens, P. H.; Wilson, K. R. A Computer Simulation Method for the Calculation of Equilibrium Constants for the Formation of Physical Clusters of Molecules: Application to Small Water Clusters. *J. Chem. Phys.* **1982**, *76*, 637.
(69) Mukamel, S. *Principles of Nonlinear Optical Spectroscopy*; Oxford University Press: New York, 1995.
(70) Hamm, P.; Zanni, M. T. *Concepts and Methods of 2D Infrared Spectroscopy*; Cambridge University Press: Cambridge, U.K., 2011.
(71) Petit, A. S.; Subotnik, J. E. How to Calculate Linear Absoprtion Spectra with Lifetime Broadening Using Fewest Switches Surface Hopping Trajectories: A Simple Generalization of Ground-State Kubo Theory. *J. Chem. Phys.* **2014**, *141*, 014107.
(72) Vegte, C. P. v. d.; Dijkstra, A. G.; Knoester, J.; Jansen, T. L. C. Calculating Two-Dimensional Spectra with the Mixed Quantum-Classical Ehrenfest Method. *J. Phys. Chem. A* **2013**, *117*, 5970−5980.
(73) Hochstrasser, R. M. Two-Dimensional IR-Spectroscopy: Polarization Anisotropy Effects. *Chem. Phys.* **2001**, *266*, 273−284.
(74) Papiz, M. Z.; Prince, S. M.; Howard, T.; Cogdell, R. J.; Isaacs, N. W. The Structure and Thermal Motion of the B800−850 LH2 Complex from Rps.acidophila at 2.0A Resolution and 100K: New Structural Features and Functionally Relevant Motions. *J. Mol. Biol.* **2003**, *326*, 1523−1538.
(75) Koolhaas, M. H. C.; van der Zwan, G.; Frese, R. N.; van Grondelle, R. Red Shift of the Zero Crossing in the CD Spectra of the LH2 Antenna Complex of Rhodopseudomonas Acidophila: A Structure-Based Study. *J. Phys. Chem. B* **1997**, *101*, 7262−7270.
(76) Lioulia, V.; Valkunas, L.; van Grondelle, R. Excitons in Chains of Dimers. *J. Phys. Chem. B* **1997**, *101*, 7343−7349.
(77) Lee, H.; Cheng, Y. C.; Fleming, G. R. Coherence Dynamics in Photosynthesis: Protein Protection of Excitinic Coherence. *Science* **2007**, *316*, 1462−1465.
(78) Kunz, R.; Timpmann, K.; Southall, J.; Cogdell, R. J.; Freiberg, A.; Köhler, J. Single-Molecule Spectroscopy Unmasks the Lowest Exciton State of B850 Assembly in LH2 from Rps. acidophila. *Biophys. J.* **2014**, *106*, 2008−2016.
(79) Dahlbom, M.; Pullerits, T.; Mukamel, S.; Sundström, V. Exciton Delocalization in the B850 Light-Harvesting Complex: Comparison of Different Measures. *J. Phys. Chem. B* **2001**, *105*, 5515−5524.
(80) Moix, J. M.; Yang, Z.; Cao, J. Equilibrium-Reduced Density Matrix Formulations: Influence of Noice, Disorder, and Temperature on Localization in Excitonic Systems. *Phys. Rev. B* **2012**, *85*, 115412.
(81) Zhang, W. M.; Meier, T.; Chernyak, V.; Mukamel, S. Exciton-Migration and Three-Pulse Femtosecond Optical Spectroscopy of Photosynthetic Antenna Complexes. *J. Chem. Phys.* **1998**, *108*, 7763−7774.
(82) Meier, T.; Chernyak, V.; Mukamel, S. Femtosecond Photon Echoes in Molecular Aggregates. *J. Chem. Phys.* **1997**, *107*, 8759−8774.
(83) Mostovoy, M.; Knoester, J. Statistics of Optical Spectra from Single-Ring Aggregates and Its Application to LH2. *J. Phys. Chem. B* **2000**, *104*, 12355−12364.

DOI: 10.1021/jp509247p
J. Phys. Chem. B 2015, 119, 1302−1313

(84) Koolhaas, M. H. C.; Frese, R. N.; Fowler, G. J. S.; Bibby, T. S.; Georgakopoulou, S.; van der Zwan, G.; Hunter, C. N.; van Grondelle, R. Identification of the Upper Exciton Component of the B850 Bacteriochlorophylls of the LH2 Antenna Complex, Using a B800-Free Mutant of Rhodobacter Sphaeroides. *Biochemistry* **1998**, *37*, 4693−4698.
(85) Georgakopoulou, S.; Frese, R. N.; Johnson, E.; Koolhaas, C.; Cogdell, R. J.; van Grondelle, R.; van der Zwan, G. Absorption and CD Spectroscopy and Modeling of Various LH2 Complexes from Purple Bacteria. *Biophys. J.* **2002**, *82*, 2184−2197.
(86) Matsushita, M.; Ketelaars, M.; van Oijen, A. M.; Köhler, J.; Aartsma, T. J.; Schmidt, J. Spectrosopy on the B850 Band of Individual Light-Harvesting 2 Complexes of Rhodopsudomonas Acidophila II. Exciton States of an Elliptically Deformed Ring Aggregate. *Biophys. J.* **2001**, *80*, 1604−1614.
(87) Heřman, P.; Zapletal, D.; Kabrhel, P. Simulation of Emission Spectra for LH2 Ring: Fluctuations in Radial Positions of Molecules. In *Recent Advances in Mathematical Methods in Applied Sciences*; Institute for Natural Sciences and Engineering: Saint Petersburg, Russia, 2014; pp 98−101.
(88) Jansen, T. L. C.; Knoester, J. Waiting time dynamics in two-dimensional infrared spectroscopy. *Acc. Chem. Res.* **2009**, *42*, 1405−1411.
(89) Dijkstra, A. G.; Jansen, T. L. C.; Knoester, J. Localization and Coherent Dynamics of Excitons in the Two-Dimensional Optical Spectrum of Molecular J-Aggregates. *J. Chem. Phys.* **2008**, *128*, 164511.
(90) Bakalis, L. D.; Knoester, J. Pump-Probe Spectroscopy and the Exciton Delocalization Length in Molecular Aggregates. *J. Phys. Chem. B* **1999**, *103*, 6620−6628.
(91) Freiberg, A.; Rätsep, M.; Timpmann, K.; Trinkunas, G.; Woodbury, N. W. Self-Trapped Excitons in LH2 Antenna Complexes between 5K and Ambiant Temperature. *J. Phys. Chem. B* **2003**, *107*, 11510−11519.
(92) Pajusalu, M.; Rätsep, M.; Trinkunas, G.; Freiberg, A. Davydov Splitting of Excitons in Cyclic Bacteriochlorophyll a Nanoaggregates of Bacterial Light-Harvesting Complexes between 4.5 and 263 K. *ChemPhysChem* **2011**, *12*, 634−644.
(93) Gelzinis, A.; Abramavicius, D.; Valkunas, L. Non-Markovian Effects in Time-Resolved Fluorescense Spectrum of Molecular Aggregates: Tracing Polaron Transformation. *Phys. Rev. B* **2011**, *84*, 245430.
(94) Hess, S.; Feldchtein, F.; Babin, A.; Nurgaleev, I.; Pullerits, T.; Sergeev, A.; Sundstrom, V. Femtosecond Energy Transfer Within the LH2 Peripheral Antenna of the Photosynthetic Purple Bacteria *Rhodobacter Spaeroides* and *Rhodopseudomonas Palustris LL*. *Chem. Phys. Lett.* **1993**, *216*, 247−257.
(95) Schreve, A. P.; Trautman, J. K.; Frank, H. A.; Owens, T. G.; Albrecht, A. C. Femtosecond Energy-Transfer Processes in the B800−850 Light-Harvesting Complex of Rhodobacter Sphaeroides 2.4.1. *Biochem. Biophys. Acta.* **1991**, *1058*, 280.
(96) Humphrey, W.; Dalke, A.; Schulten, K. VMD - Visual Molecular Dynamics. *J. Mol. Graphics* **1996**, *14*, 33−38.

DOI: 10.1021/jp509247p
J. Phys. Chem. B 2015, 119, 1302−1313